Molecular Therapy
Original Article

Extracellular Vesicles Containing IL-4 Modulate Neuroinflammation in a Mouse Model of Multiple Sclerosis

Giacomo Casella,[1] Federico Colombo,[1] Annamaria Finardi,[1] Hélène Descamps,[2] Gerard Ill-Raga,[1] Antonello Spinelli,[3] Paola Podini,[4] Mattia Bastoni,[1] Gianvito Martino,[2] Luca Muzio,[2] and Roberto Furlan[1]

[1]Clinical Neuroimmunology Unit, Department of Neuroscience, Institute of Experimental Neurology (InSpe), San Raffaele Scientific Institute, 20132 Milan, Italy; [2]Neuroimmunology Unit, Department of Neuroscience, Institute of Experimental Neurology, San Raffaele Scientific Institute, 20132 Milan, Italy; [3]Experimental Imaging Centre, San Raffaele Scientific Institute, 20132 Milan, Italy; [4]Department of Neuroscience, Institute of Experimental Neurology, San Raffaele Scientific Institute, 20132 Milan, Italy

Extracellular vesicles (EVs) play a major role in cell-to-cell communication in physiological and pathological conditions, and their manipulation may represent a promising therapeutic strategy. Microglia, the parenchymal mononuclear phagocytes of the brain, modulate neighboring cells also through the release of EVs. The production of custom EVs filled with desired molecules, possibly targeted to make their uptake cell specific, and their administration in biological fluids may represent a valid approach for drug delivery. We engineered a murine microglia cell line, BV-2, to release EVs overexpressing the endogenous "eat me" signal Lactadherin (Mfg-e8) on the surface to target phagocytes and containing the anti-inflammatory cytokine IL-4. A single injection of 10^7 IL-4$^+$Mfg-e8$^+$ EVs into the cisterna magna modulated established neuroinflammation and significantly reduced clinical signs in the mouse model of multiple sclerosis, experimental autoimmune encephalomyelitis (EAE). Injected IL-4$^+$Mfg-e8$^+$ EVs target mainly phagocytes (i.e., macrophages and microglia) surrounding liquoral spaces, and their cargo promote the upregulation of anti-inflammatory markers chitinase 3-like 3 (ym1) and arginase-1 (arg1), significantly reducing tissue damage. Engineered EVs may represent a biological drug delivery tool able to deliver multiple functional molecules simultaneously to treat neuroinflammatory diseases.

INTRODUCTION

Extracellular vesicles (EVs) are small membrane particles released by all cell types.[1,2] EVs are usually subdivided in smaller particles called exosomes (10–100 nm), larger vesicles called microvesicles (100–1,000 nm), and apoptotic bodies (>1,000 nm).[2,3] EVs have been recently characterized as mediators of intercellular communication, and their role has been extensively investigated in physiology and disease.[1,3] It has been reported that EVs can deliver different kind of molecules, such as nucleic acids and proteins, which often influence the phenotype of recipient cells. To induce a biological effect, EVs need to interact with target cells, either directly with the plasma membrane or with the endosomal membrane after cellular uptake.[4,5] In fact, there are different mechanisms of EVs' content delivery inside cells, depending, for example, on EV size range, releasing rate, and recipient cell origin.[6] Further, EVs can simultaneously deliver several different signals to a cell. We need to better understand the interaction between EVs and recipient cells, in physiology and pathology, to improve the design of EVs as biological vectors for the delivery of therapeutics.[7,8]

All CNS resident cells tested release EVs *in vitro* and *in vivo*.[9] EVs are involved in shuttling signals between neighboring cells within the CNS,[10] regulating various physiological and pathological processes, including development, synaptic neurotransmission, neurodegeneration, and CNS tumor progression. EVs participate in immunologic surveillance, information exchange, and epigenetic modulation, and they may contribute to the spreading of pathological molecules in some neurodegenerative and neuroinflammatory diseases.[11]

We have shown in the past, in mice and humans, that microglia EV trafficking is increased during multiple sclerosis and its mouse model, experimental autoimmune encephalomyelitis (EAE), and that microglia-derived EVs are preferentially uptaken by other microglia.[12]

We have also shown, in both murine and primate EAE models, that CNS delivery of the anti-inflammatory cytokine interleukin-4 (IL-4) through gene therapy is extremely efficient in treating ongoing neuroinflammation.[13,14]

Here we report that EVs of microglial origin expressing the endogenous "eat me" signal Lactadherin (Mfg-e8), injected in the cisterna magna during EAE, are targeted to CNS phagocytes[15,16] and can

Received 20 March 2018; accepted 25 June 2018;
https://doi.org/10.1016/j.ymthe.2018.06.024.

Correspondence: Roberto Furlan, Clinical Neuroimmunology Unit, Department of Neuroscience, Institute of Experimental Neurology (InSpe), San Raffaele Scientific Institute, Via Olgettina 58, 20132 Milan, Italy.
E-mail: furlan.roberto@hsr.it

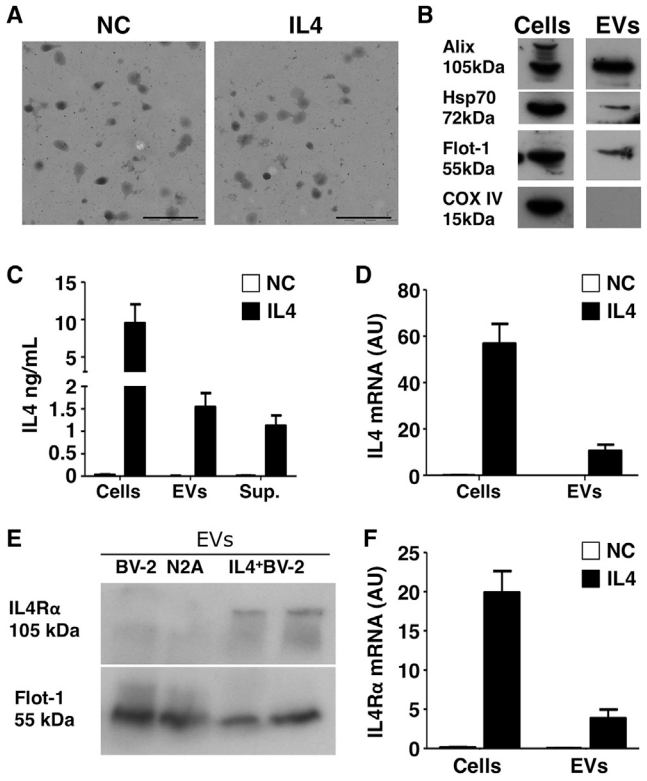

Figure 1. IL-4$^+$ EV Characterization

(A) TEM analysis of a representative EV pellet derived from IL-4$^+$BV-2 cells (IL-4) and untransfected BV-2 cells as negative control (NC) (n = 3). Scale bars, 500 nm. (B) Western blot analysis of EVs from IL-4$^+$BV-2 cells for EV markers (Alix, Hsp70, Flotillin-1, and COX-IV) (n = 3). (C) Measurement, by ELISA, of IL-4 in IL-4$^+$BV-2 cell lysates (cells), IL-4$^+$ EVs (EVs), and IL-4$^+$BV-2 supernatants (sup.). Untransfected BV-2 cells were used as a negative control (NC) (n = 5). Bars are mean values ± SD. (D) IL-4 mRNA detected by RT-PCR in IL-4$^+$BV-2 cells and IL-4$^+$ EVs (IL-4) as compared to untransfected BV-2 cells (NC) (n = 5). Values are expressed as a.u. and bars represent mean values ± SD. (E) WB for IL-4Rα on EVs from untransfected BV-2 cells (BV-2), from the N2A neuronal cell line (N2A), and from IL-4$^+$ BV-2 cells (IL-4$^+$ BV-2) (n = 3). Protein load was controlled using flotilin-1 (Flot-1). (F) RT-PCR for IL-4Rα mRNA in EVs from untransfected BV-2 cells (NC) and IL-4$^+$BV-2 cells (IL-4), and corresponding parental cells (n = 4). Values are expressed as a.u. and bars represent mean values ± SD. Blots in (B) and (E) have been cropped. Full pictures are presented in Figure S7.

deliver IL-4 and Cre-recombinase. We describe their ability to influence recipient cells' phenotype *in vitro* and *in vivo* and to modulate ongoing EAE.

RESULTS

Production and Characterization of IL-4-Containing EVs

We transfected murine BV-2 microglia cells with a plasmid coding for murine IL-4, and we used EVs released by untransfected donor cells as a negative control (NC). After 48 hr, we collected both exosomes and microvesicles (MVs) using the procedure described in Figure S1A. We characterized IL-4$^+$ EVs (IL-4) by electron microscopy (Figure 1A), western blot (WB) (Figure 1B), tunable resistive pulse sensing (TRPS) (Figures S1B and S1C), and flow cytometry (Figures S1D and S1E). We found that EVs from IL-4$^+$ BV-2 contain IL-4 protein (Figure 1C), IL-4 mRNA (Figure 1D), IL-4 receptor alpha (IL-4Rα) mRNA, and IL-4Rα protein (Figures 1E and 1F).

Administration of IL-4-Containing EVs Induces Anti-inflammatory Marker Expression in Recipient Myeloid Cells

We next administered IL-4$^+$ EVs to recipient myeloid cells *in vitro*. Administration of IL-4$^+$ EVs is well tolerated, as demonstrated by MTT toxicity assay (Figure S2A). Starting 4 hr after administration, cells receiving IL-4$^+$ EVs upregulated anti-inflammatory markers, such as arginase-1 (arg1) and chitinase 3-like 3 (ym1), with a slightly delayed kinetic as compared to recombinant IL-4 (Figures S2B and S2C). The effect was directly proportional to the number of EVs administered (Figures 2A and 2B). To exclude IL-4 carryover, we depleted soluble IL-4 outside EVs with a specific antibody, and we found no effect on the induction of arg1 and ym1 mRNAs (Figures 2C and 2D). We confirmed the upregulation of anti-inflammatory markers, such as CD206 and arg1, and the decrease of the pro-inflammatory marker iNOS, both at the protein and mRNA levels, in primary microglia (Figures 2E–2G) and in peritoneal macrophages (Figures S2D–S2F). IL-4$^+$ EVs display, therefore, a polarizing ability similar to recombinant murine IL-4 in recipient myeloid cells.

IL-4$^+$ EV-Induced Upregulation of Anti-inflammatory Markers Is STAT6 Dependent

Results obtained upon IL-4 depletion in the EV-containing supernatant and the strict dose dependence suggest that EV content is responsible for the IL-4$^+$ EV effect on recipient myeloid cells. Indeed, co-incubation of myeloid cells with an IL-4 receptor-blocking antibody inhibited the activity of recombinant IL-4, but not of IL-4$^+$ EVs (Figures 3A and 3B). Administration of IL-4$^+$ EVs, however, caused activation of the classical IL-4 pathway, as demonstrated by the phosphorylation of STAT6 (Figures 3C and 3D). Furthermore, the transcription of anti-inflammatory markers induced by IL-4$^+$ EVs is blocked in the presence of a STAT6 inhibitor (Figures 3E and 3F).

Mfg-e8 Expression on EVs Increases Signal Delivery

To increase EV uptake by phagocytes, we obtained IL-4$^+$ EVs also by BV-2 stably expressing the eat me signal Mfg-e8, also known as lactadherin.[15] IL-4$^+$Mfg-e8$^+$ EVs (Figures S3A–S3C) did not display morphological alterations (Mfg-e8), compared to non-targeted EVs (EVs) (Figure S3A), or differences in their number (Figure S3C) or IL-4 content (Figure S3D), compared to IL-4$^+$Mfg-e8$^-$ EVs. Further, IL-4$^+$Mfg-e8$^+$ EVs displayed increased ability to induce ym1 and arg1 mRNA, as compared to IL-4$^+$ EVs, in recipient cells (Figures 3G and 3H). Mfg-e8$^+$ EVs without IL-4 did not display any effect (Figures S3E and S3F). We used recombinant αvβ5 integrin to inhibit Mfg-e8 since it is known that lactadherin activity is dependent on binding to integrin receptors.[15] In fact, in the presence of recombinant αvβ5 integrin IL-4$^+$Mfg-e8$^+$ EVs, biological effect was significantly reduced, as shown for arg1 mRNA levels (Figure S3E),

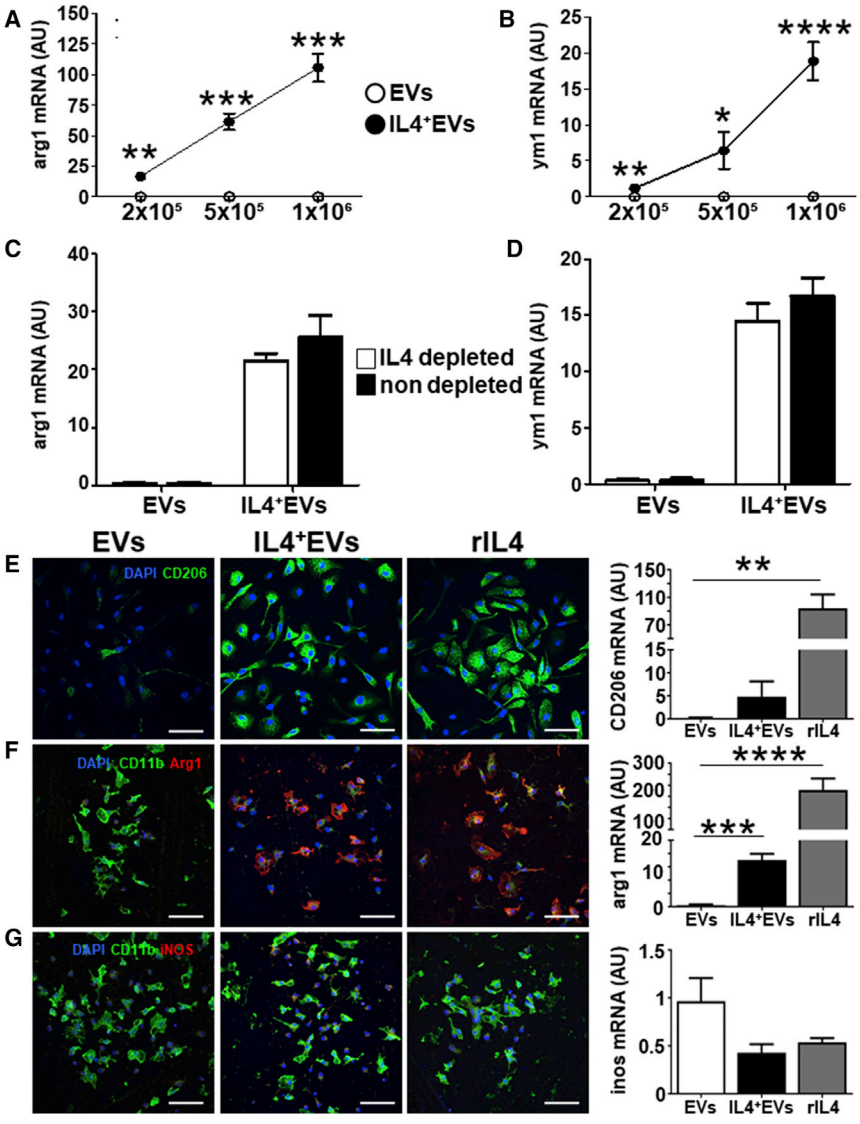

Figure 2. IL-4⁺ EVs Modulate Recipient Cells *In Vitro*

(A and B) RT-PCR analysis for arginase-1 (arg1) (A) and ym1 (B) in recipient BV-2 cells, treated, as indicated on the x axis, with 2×10^5, 5×10^5, and 1×10^6 IL-4⁺ EVs (IL-4⁺ EVs, closed dots) or IL-4⁻ EVs (EVs, open dots), for 8 hr (n = 4). Values are expressed as a.u. and data points represent mean values ± SD. (C and D) To exclude IL-4 carryover, 1×10^6 IL-4⁺ EVs depleted of extra-vesicular IL-4 by treatment with anti-IL-4 antibody and protein G precipitation (open bars), or non-depleted 1×10^6 IL-4⁺ EVs (closed bars), were added to recipient BV-2 (n = 4), arg1 (C), and ym1 (D). Values are expressed as a.u. and bars represent mean values ± SD and were analyzed with two-tailed unpaired t test, *$p < 0.005$, **$p < 0.001$, ***$p < 0.0001$, and ****$p < 0.00001$. (E–G) IL-4⁺ EVs' effect on primary microglia phenotype. Immunofluorescence is shown for CD206 (green, E; Arg1, red, F; iNOS, red, G) in primary microglia treated with IL-4⁻ EVs, IL-4⁺ EVs (EV:cell ratio 3.5:1), and rIL-4 (20 ng/mL) for 12 hr (n = 5). Along with Arg1 and iNOS, CD11B (green) was used to identify myeloid cells and DAPI (blue) for nuclei. Levels of the corresponding mRNA (CD206, arg1, and ym1), measured by RT-PCR in the same cultures, are shown in the bar graphs on the right (n = 5). Gapdh was used as a housekeeping gene. Ym1, arg1, and inos mRNA levels are expressed as a.u.; data are expressed as means ± SD and were analyzed with the one-way ANOVA test (**$p < 0.001$, ***$p < 0.0001$, and ****$p < 0.00001$, E–G).

while no differences for inos mRNA levels were detected in all conditions (Figure S3F).

Myeloid Phagocytes Uptake EVs by Phagocytosis, and EV Delivery Content Is Affected by Lysosome Activity

Microglia and macrophages are phagocytes with a well-developed lysosomal apparatus that can influence EVs' content delivery.[17] As suggested by the activity of Mfg-e8, these cells may uptake EVs by phagocytosis (Figure S4A). Blocking lysosomal activity in recipient phagocytes with *Bafilomycin* (1 μM), we increased EVs' content delivery, as shown in Figures S4B–S4D. Moreover, *Bafilomycin* treatment for 3, 6, or 9 hr significantly increased the IL-4⁺ EV-induced transcription of the anti-inflammatory markers arg1 and ym1 (Figures 3I and 3J; Figures S4E–S4G), suggesting that EVs' cargo is partially destroyed by lysosomes in physiological conditions and that its intracellular delivery is crucial to modulate recipient cells.

EVs Injected in the Mouse Cisterna Magna Are Uptaken by Myeloid Cells and Astrocytes

To characterize EV fate *in vivo*, we prepared EVs from BV-2 transfected with a plasmid coding for Cre recombinase, and we injected 10^7 Cre⁺Mfg-e8⁺ EVs into the cisterna magna of healthy R26-stop-EYFP reporter mice, as described previously.[14] Cre⁺Mfg-e8⁺ EVs can spread inside the liquoral space and reach the spinal cord up to the thoracic region. We found that ependymal and leptomeningeal cells surrounding the brain and the spinal cord recombine the reporter gene locus and become fluorescent (Figures 4B, 4D, 4F, and 4H). Recombination of parenchymal cells is a rare event, suggesting that Cre⁺Mfg-e8⁺ EVs cannot efficiently diffuse into the brain or spinal cord parenchyma. Double staining showed that most cells uptaking Cre⁺Mfg-e8⁺ EVs are Iba1⁺ myeloid cells (Figures 4B–4D) and a few GFAP⁺ astrocytes close to liquoral spaces, both in brain and spinal cord (Figures 4F–4H). We confirmed these findings using EVs loaded with luciferase and *in vivo* bioluminescence imaging (BLI) (Figure S5). EVs containing luciferase were quantified by TRPS (Figure S5A), and total luminescence was analyzed from 10^7 EVs *in vitro* (Figure S5B). We found that intravenous injection never resulted in localization of the luminescent signal in the brain (data not shown), while intracisternal injection of Mfg-e8⁺ EVs loaded with luciferase resulted in

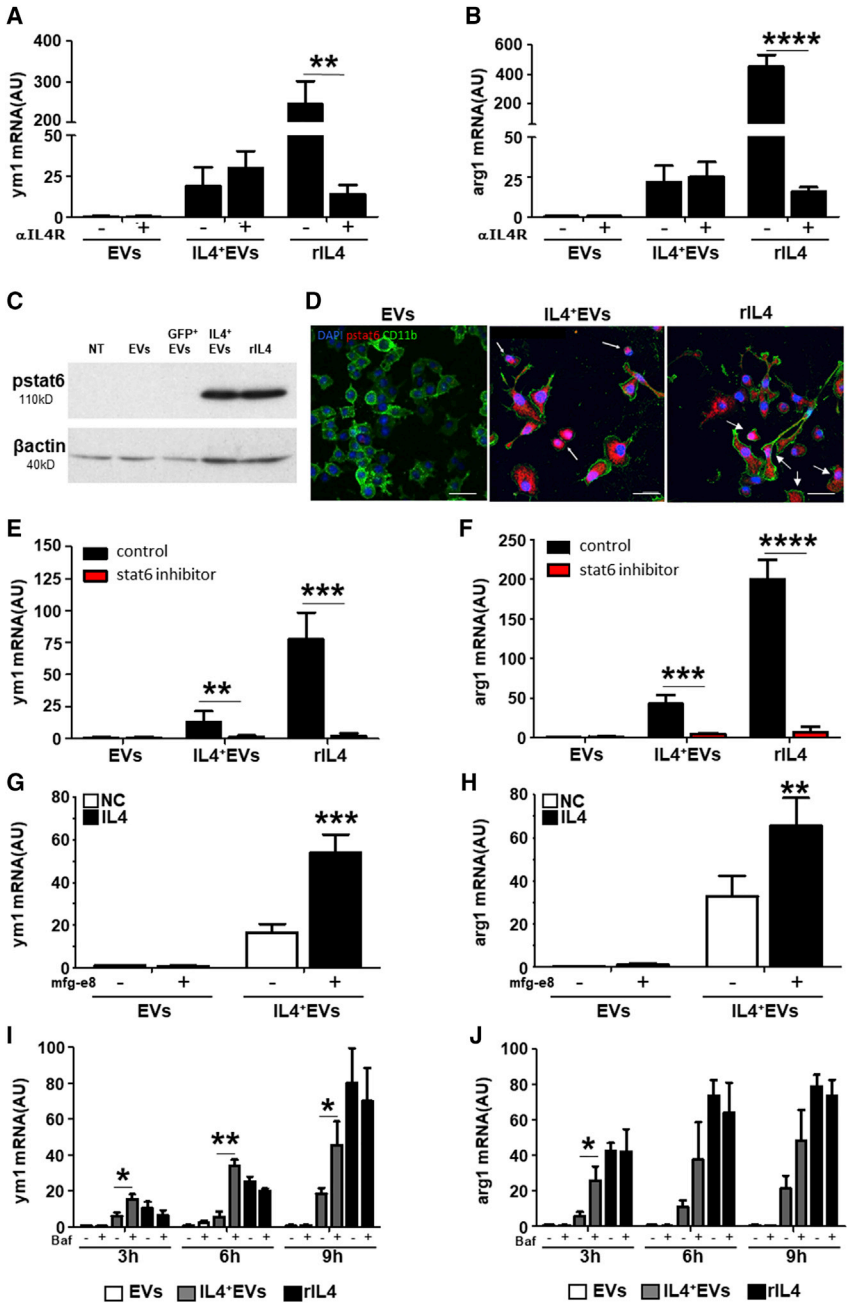

Figure 3. IL-4$^+$ EV Signaling Occurs Inside the Cell and Is Dependent on STAT6 and Lysosome Efficiency

(A and B) RT-PCR analysis for ym1 (A) and arginase-1 (arg1) (B) in recipient BV-2 cells treated with 1 × 10^6 IL-4$^-$ EVs (EVs), IL-4$^+$ EVs (IL-4$^+$ EVs), or recombinant IL-4 (20 ng/mL, rIL-4) for 8 hr. IL-4Rα-neutralizing antibody (1 μg/mL) was added 1 hr before treatment (n = 4). Gapdh was used as a housekeeping gene. ym1 and arg1 mRNA levels are expressed as a.u.; data are expressed as mean ± SD and were analyzed with two-tailed unpaired t test (**p < 0.001 and ****p < 0.00001). (C) Western blot for phosphorylated STAT6 (pstat6) in untreated BV-2 cells (NT) or BV-2 cells receiving 1 × 10^6 IL-4$^-$ EVs (EVs), GFP$^+$ EVs, IL-4$^+$ EVs, or 20 ng/mL recombinant IL-4 (rIL-4) for 4 hr (n = 3). Predicted molecular weight (MW) of pSTAT6 is 110 kDA. Protein load was controlled using β-actin (MW = 40 kDa). (D) Immunofluorescence for phosphorylated pstat6 (red, pstat6), CD11b (green), and nuclei (DAPI) in BV-2 cells receiving 1 × 10^6 IL-4$^-$ EVs (EVs), IL-4$^+$ EVs, or rIL-4 (20 ng/mL) for 4 hr (n = 4). (E and F) The stat6 inhibitor AS1517499 (10 μM; red bars) or control medium (control; black bars) was added 1 hr before treatment of recipient BV-2 cells with IL-4$^-$ EVs, IL-4$^+$ EVs, or rIL-4. The reaction was blocked after 5 hr, and RT-PCR for ym1 and arg1 was performed on recipient BV-2 cells (n = 5). ym1 (E) and arg1 (F) mRNA levels are expressed as a.u.; data are expressed as means ± SD and were analyzed with unpaired t test two-tailed (**p < 0.001, ***p < 0.0001, and ****p < 0.00001). (G and H) IL-4$^+$Mfg-e8$^+$ EVs are more efficient in modulating gene transcription compared to IL-4$^+$ EVs in recipient BV-2 cells. RT-PCR is shown for ym1 (G) and arg1 (H) mRNA transcripts from BV-2 cells treated with 1 × 10^6 IL-4$^-$ or IL-4$^+$ EVs expressing or not Mfg-8, for 8 hr (n = 5). Gapdh was used as a housekeeping gene. mRNA levels are expressed as a.u.; data are expressed as means ± SD and were analyzed with two-tailed unpaired t test (**p < 0.001 and ***p < 0.0001). (I and J) *Bafilomycin* (1 μM) was added for 1 hr before treatment of recipient BV-2 cells with 1 × 10^6 IL-4$^-$ EVs (white bars), IL-4$^+$ EVs (gray bars), or rIL-4 (20 ng/mL; black bars) for 3, 6, and 9 hr, and RT-PCR for ym1 (I) and arg1 (J) was performed on recipient BV-2 cells (n = 5). ym1 and arg1 mRNA levels are expressed as a.u.; data are expressed as means ± SD and were analyzed with unpaired t test two tailed (*p < 0.01 and **p < 0.001). Blots (C) have been cropped. Full picture is presented in Figure S7.

sustained BLI signal, specifically in the brain, for at least 5 days (Figures S5C–S5F).

Intrathecal Injection of IL-4$^+$Mfg-e8$^+$ EVs Protects from Neuroinflammation

To evaluate the therapeutic potential of IL-4$^+$Mfg-e8$^+$ EVs *in vivo*, we injected 10^7 IL-4$^+$Mfg-e8$^+$ EVs into the cisterna magna of EAE mice the day of disease clinical onset (Figure 5A). A single intrathecal injection of 10^7 IL-4$^+$Mfg-e8$^+$ EVs resulted in significant protection from clinical (Figures 5A and 5B) and neuropathological signs of the disease (Figures 5D–5F). The injection of broken IL-4$^+$ EVs, destroyed by freezing and thawing, was ineffective, suggesting that IL-4$^+$ EVs' effect is dependent on their content (Figure S6A). We also tried to prolong EAE monitoring, finding that IL-4$^+$Mfg-e8$^+$ EV effect persists up to 30 days after injection (Figure S6B). We found detectable levels of IL-4 protein in the cerebrospinal fluid (CSF) of IL-4$^+$Mfg-e8$^+$ EV-treated mice 14 days after injection (Figure 5B; Figure S6C), a time largely exceeding the predicted half-life of the IL-4 protein,[18] but possibly also of the IL-4 mRNA. IL-4 increase in the CSF was not significant at

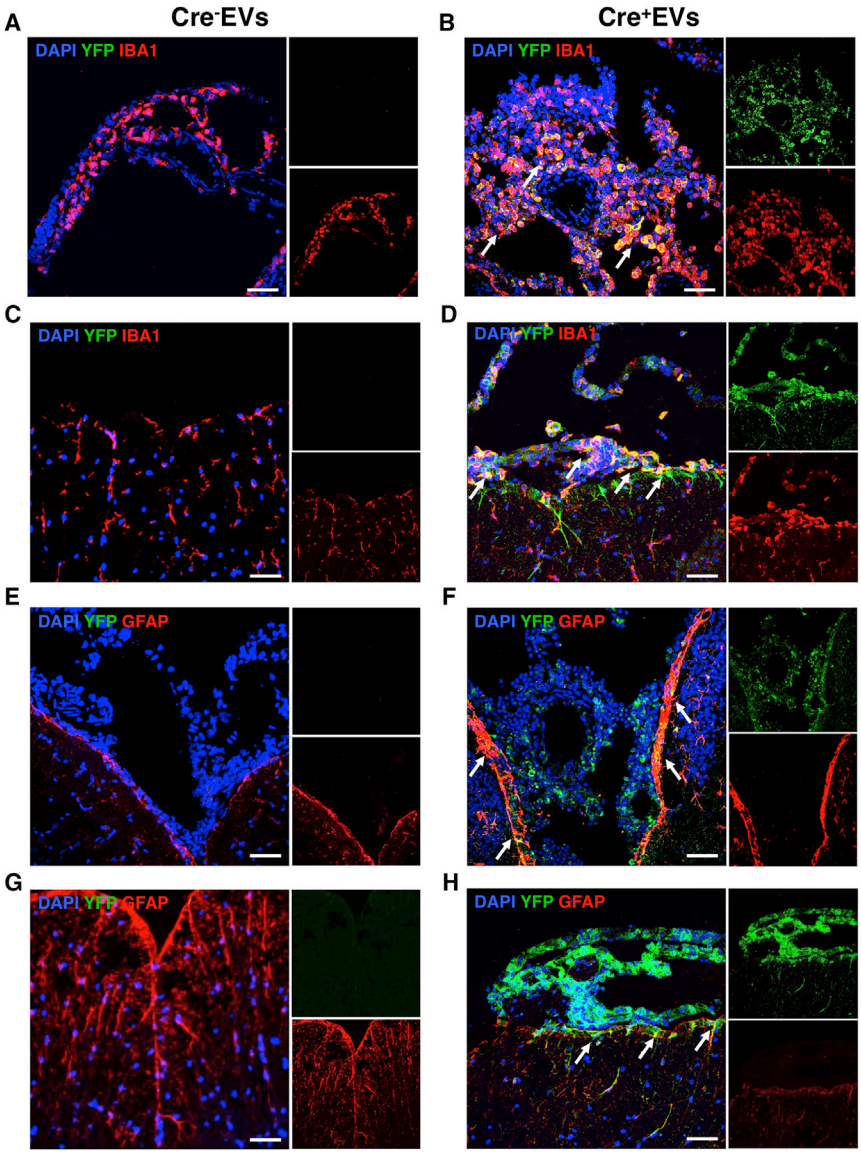

Figure 4. Mfg-e8⁺ EV Delivery *In Vivo*

R26-stop-EYFP reporter mice were intracisternally injected with 10^7 Mfg-e8⁺ EVs containing (Cre⁺ EVs; B, D, F, and H) or not Cre recombinase (Cre⁻ EVs; A, C, E, and G). Coronal brain (A, B, E, and F) and spinal cord sections (C, D, G, and H) were stained for YFP (green) (A–H), and for IBA1 (red; A–D) or GFAP (red; E–H) and DAPI (blue). Sections are a representation of third ventricle (A, B, E, and F) and thoracic region (C, D, G, and H). Magnification, 40×; scale bar, 50 μm; n = 3/group.

30 days after injection (Figure S6D). This suggests, however, that the delivery of IL-4⁺Mfg-e8⁺ EVs may induce a long-lasting immunomodulation, resulting in prolonged IL-4 release. Accordingly, in EAE mice treated with IL-4⁺Mfg-e8⁺ EVs, we detected a significant increase of cells expressing anti-inflammatory markers arg1 and ym1 (Figures 6A and 6B) and a parallel decrease of the pro-inflammatory marker iNOS (Figures 6C and 6D), as compared to mice injected with Mfg-e8⁺ EVs loaded with GFP (GFP⁺Mfg-e8⁺ EVs) used as a control.

IL-4⁺Mfg-e8⁺ EVs Change the Phenotype of Recipient Myeloid Cells *In Vivo*

We purified infiltrating CD11b⁺ myeloid cells and CD4⁺ T cells from the CNS of EAE mice, and we found by RT-PCR that IL-4⁺Mfg-e8⁺ EV treatment significantly decreased inos mRNA expression (Figure 6E) and increased the anti-inflammatory markers arg1 and ym1 (Figures 6F and 6G) in myeloid cells. We also measured interferon (IFN)γ, IL-17, and rorc mRNA levels in infiltrating CD4⁺ T cells (Figures 6H–6J). Only IL-17 mRNA was significantly downregulated by treatment (Figure 6I).

Polarization Induced by IL-4⁺Mfg-e8⁺ EVs Is Dependent on Intracellular Cargo Delivery

To confirm that the expression of anti-inflammatory markers in myeloid cells is dependent on cargo delivery by engineered EVs, we plated IL-4⁺Cre⁺Mfg-e8⁺ EVs on recipient R26stop-YFP macrophages. Indeed, cells that were cultured in the presence of IL-4⁺Mfg-e8⁺ Cre⁺ EVs co-expressed CD206 and YFP (Figure 7A). *In vivo*, we injected 10^7 IL-4⁺Mfg-e8⁺ Cre⁺ EVs into R26stop-tdTomato EAE mice, and we found an upregulation of the M2 marker CD206 only in myeloid cells (Iba1⁺) that had recombined the reporter locus (Figure 7C). This suggests, *in vitro* and *in vivo*, that intracellular cargo delivery is the crucial mechanism to modulate the recipient cells' phenotype, as suggested also by the fact that administration of IL-4⁺Mfg-e8⁺ EVs broken by repeated freezing and thawing did not inhibit disease (Figure S6A).

DISCUSSION

EVs are being developed as a drug delivery tool for many diseases,[6] including neurological disorders, despite the fact that the biology concerning both their release and communication modalities remains to be fully elucidated. The possibility to hack EV-mediated intercellular communication, delivering a message of choice, opens the possibility of new therapeutic strategies for many applications. The ability to deliver multiple functional molecules in different biological districts, via body fluids, without showing immunogenicity, makes EVs candidate alternatives to liposomes or artificial nanoparticles.[19]

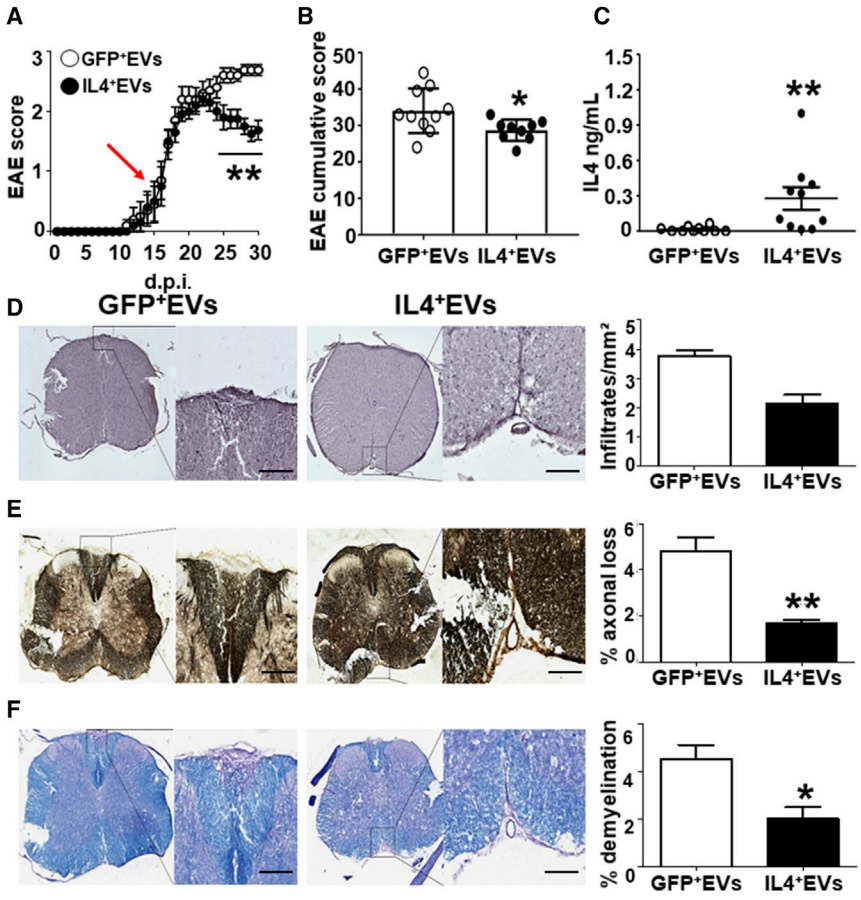

Figure 5. IL-4⁺ Mfg-e8⁺ EV Injection Modulates EAE and Protects EAE Mice from Tissue Damage

(A) EAE mice were intracisternally injected, at clinical onset (red arrow), with 10^7 Mfg-8⁺ EVs containing GFP (GFP⁺ EVs, open dots) or IL-4 (IL-4⁺ EVs, closed dots). Dots represent mean daily EAE score; data are expressed as means ± SEM and were analyzed with two-way ANOVA Bonferroni test (**$p < 0.005$). n = 10/group. (B) EAE cumulative score of the same mice intracisternally injected with 10^7 EVs containing GFP (GFP⁺ EVs, open dots) or IL-4 (IL-4⁺ EVs, closed dots) (n = 10). (C) In the same mice, IL-4 protein was measured in the CSF by ELISA. Data are expressed as means ± SEM and were analyzed with two-tailed unpaired t test (**$p < 0.01$) (n = 10). (D–F) Histological analysis of the spinal cord of EAE mice injected with 10^7 GFP⁺Mfg-e8⁺ (GFP⁺ EVs) or IL-4⁺Mfg-e8⁺ EVs (IL-4⁺ EVs) (n = 5). Adjacent sections are stained to detect inflammatory infiltrates (H&E, D), axonal loss (Bielshowsky, E), and demyelination (Kluver Barrera, F). Magnification, 20×; n = 5/group; scale bar, 100 μm. Column bars represent mean values ± SD; *$p < 0.05$ and **$p < 0.001$ (two-tailed unpaired t test).

We describe here that EVs released by a murine microglia cell line can be loaded with the desired protein (i.e., IL-4, Cre recombinase, and luciferase) and targeted preferentially to phagocytes, a cell type involved in numerous pathologies, including tumors and neurodegenerative disorders, by the expression of Mfg-e8 on their surface. We provide evidence that EVs' ability to modulate recipient cells depends on how EVs are internalized, on their cargo, and on its capacity to escape lysosomal destruction. This clearly provides indications on the nature of signals that it is possible to deliver efficiently through this kind of EV.

In our specific case, we used microglia BV-2 as source of EVs to increase EVs' ability to target microglia and macrophages. Previous data suggest that microglia-derived EVs are preferentially uptaken by other microglia.[12] We decided to use all EVs, namely, exosomes and microvesicles. In most reports describing EVs as a drug delivery tool, only exosomes are purified.[19,20] The choice to use the combination of exosomes and microvesicles appears to have several advantages in a therapeutic setting.[17]

IL-4⁺ EVs have induced, *in vitro*, the upregulation of anti-inflammatory markers in different myeloid cells, i.e., BV-2 cells, primary microglia, and peritoneal macrophages. WB and RT-PCR analysis confirmed the presence of both IL-4 and IL-4Rα proteins and mRNA transcripts, suggesting that EVs deliver several functional molecules simultaneously. Moreover, IL-4⁺ EVs have shown to work in a dose-dependent manner.

We demonstrated that the biological effect of IL-4⁺ EVs is mainly dependent on IL-4 inside the vesicles. IL-4⁺ EVs have been shown to deliver IL-4Rα, and we cannot exclude that IL-4 travels also already bound to its receptor on EVs. It is already described that cytokines, such as IFNγ delivered by EVs, can be found bound to their receptor.[21]

Interestingly, IL-4⁺ EVs work even in the presence of IL-4Rα inhibitor (the same does not happen for recombinant IL-4 [rIL-4]); one reason could be that IL-4 encapsulated in EVs signals through IL-4R clustered in cytosolic organelles called cortical endosomes, after their cellular uptake.[22] Experiments using a stat6 inhibitor confirmed that IL-4⁺ EVs signal through stat6.

How EVs are uptaken by recipient cells is a hot topic in the EV field. EVs can be internalized mainly by endocytosis, direct fusion, and phagocytosis, depending on many factors, such as EV origin, size, membrane proteins, and recipient cells.[4,9] Our data support the hypothesis that phagocytes, such as microglia, macrophages, and dendritic cells, may uptake EVs by phagocytosis, thus addressing them to the lysosomal compartment where they are recycled or destroyed.[4] We tried to investigate this point by using bafilomycin, a potent inhibitor of lysosome acidification.[16] In fact, in the presence of bafilomycin IL-4⁺ EVs induced a stronger effect, suggesting that lysosomes destroy a significant portion of the EVs' cargo. Since it

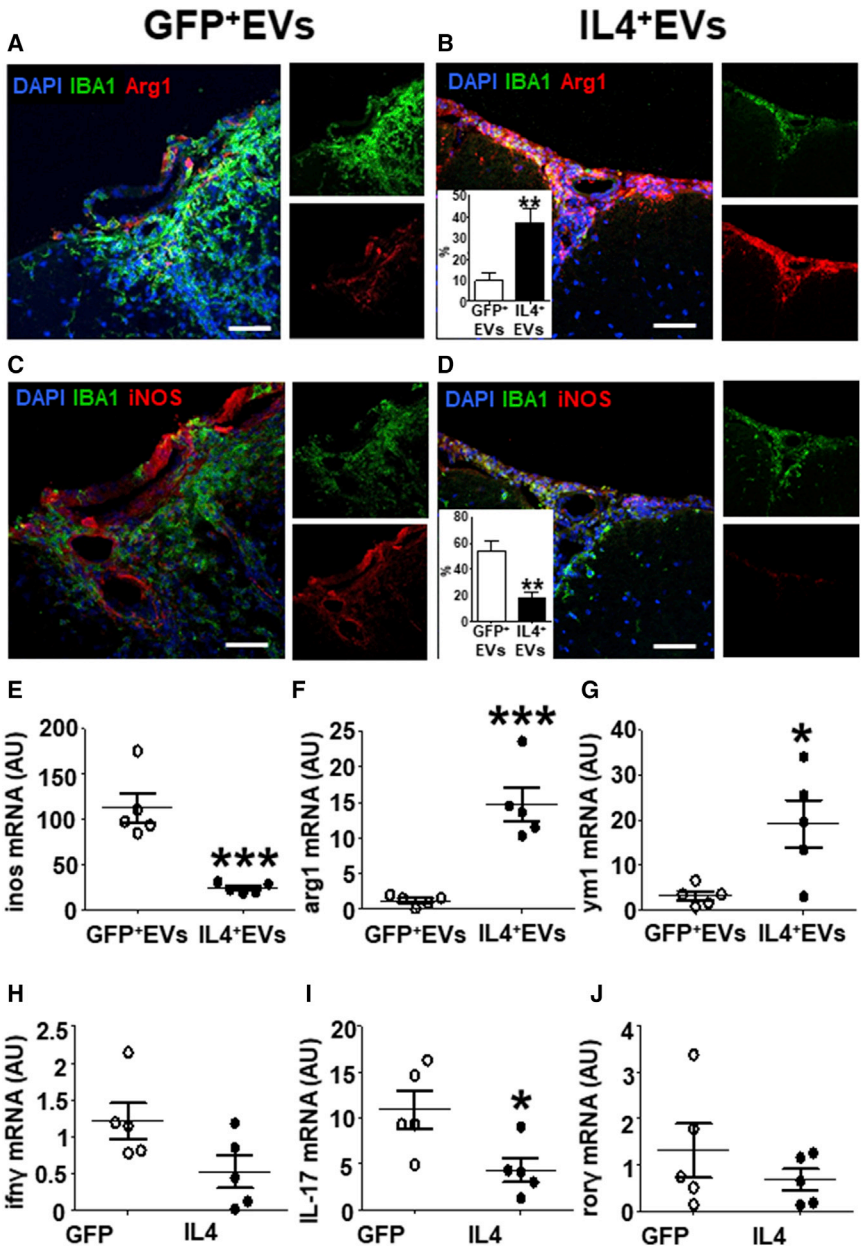

Figure 6. IL-4$^+$Mfg-e8$^+$ EV Injection in EAE Mice Induces Anti-inflammatory Markers on CNS Phagocytes

(A–D) Immunofluorescence for Arg1 (red; A and B) and iNOS (red; C and D) in spinal cord sections of EAE mice injected with 10^7 GFP$^+$ (GFP$^+$ EVs) or IL-4$^+$ Mfg-e8$^+$ EVs (IL-4$^+$ EVs) (n = 5). IBA1 (green) was used to identify myeloid cells and DAPI (blue) for nuclei. Percentage of double-positive IBA1$^+$Arg1$^+$ and IBA1$^+$iNOS$^+$ cells on total IBA1$^+$ cells are shown in the insets of (B)–(D) in IL-4-treated (closed bars) or GFP-treated (open bars) mice. Data are expressed as means ± SD and were analyzed with two-tailed unpaired t test (**p < 0.01). (E–J) RT-PCR for inos (E), arg1 (F), and ym1 mRNA (G) was performed on CNS-infiltrating CD11b$^+$ cells, whereas RT-PCR for ifnγ (H), il-17 (I), and rorγ mRNAs (J) was performed on CNS-infiltrating CD4$^+$cells from EAE mice intracisternally injected with 10^7 GFP$^+$ (GFP$^+$ EVs) or IL-4$^+$ Mfg-e8$^+$ EVs (IL-4$^+$ EVs) (n = 5). Gapdh was used as a housekeeping gene. Data are shown as a.u. and were analyzed with two-tailed unpaired t test (*p < 0.05 and ***p < 0.001).

has been already described that EVs' content may undergo endosomal escape,[9] we cannot exclude that IL-4$^+$ EVs, once entered into the cytosol, also undergo endosomal escape. The ability of EVs to target the lysosomal compartment might be exploited in the treatment of lysosomal storage disorders, although their uptake and intracellular sorting may differ in different cell types.

We used EVs overexpressing lactadherin, Mfg-e8, to exploit its ability to increase uptake of vesicles by phagocytes. In the literature, Mfg-e8 is described as an exosome marker in dendritic cells or platelets,[23] and it has been used as an adaptor protein to expose a reporter protein on EVs.[24] We describe here the use of Mfg-e8 as a signal to increase cellular targeting. EVs targeting with Mfg-e8 increased the biological effect of IL-4$^+$ EVs. On the other hand, Mfg-e8$^+$ EVs have not an intrinsic capacity to induce the M2 phenotype on recipient microglia, as demonstrated using rαVβ5 integrin blocking specifically the activity of Mfg-e8, also demonstrating its dependency on integrin receptors.[15,25]

In vivo we used mainly intracisternal injection, already well documented,[26] to deliver EVs directly into the CNS of wild-type and EAE mice. Several studies have shown intravenous (i.v.) injection as a suitable method for EV delivery in mice to target CNS-resident cells,[17,19,27,28] but we have failed to reproduce these findings. By intracisternal (i.c.) injection, EVs spread into liquoral spaces, distributing into the brain and reaching the spinal cord (until the thoracic region). We obtained similar results using viral particles in the past.[13,14] Intrathecally delivered EVs mainly interact with phagocytes that traffic through the CSF, such as infiltrating monocytes, and maybe with subpial microglia. With both intrathecally administered Cre$^+$Mfg-e8$^+$ EVs and Cre$^+$Mfg-e8$^-$ EVs, we found only sporadic recombination of the reporter gene in the CNS parenchyma, as also reported previously for exosomes injected into lateral ventricles.[29] Widespread CNS distribution has been, instead, reported by other investigators.[19,27]

EAE is an autoimmune disease where the main inflammatory process takes place in the meninges. By the injection of IL-4$^+$Mfg-e8$^+$ EVs into liquoral space, we can directly target meningeal resident cells

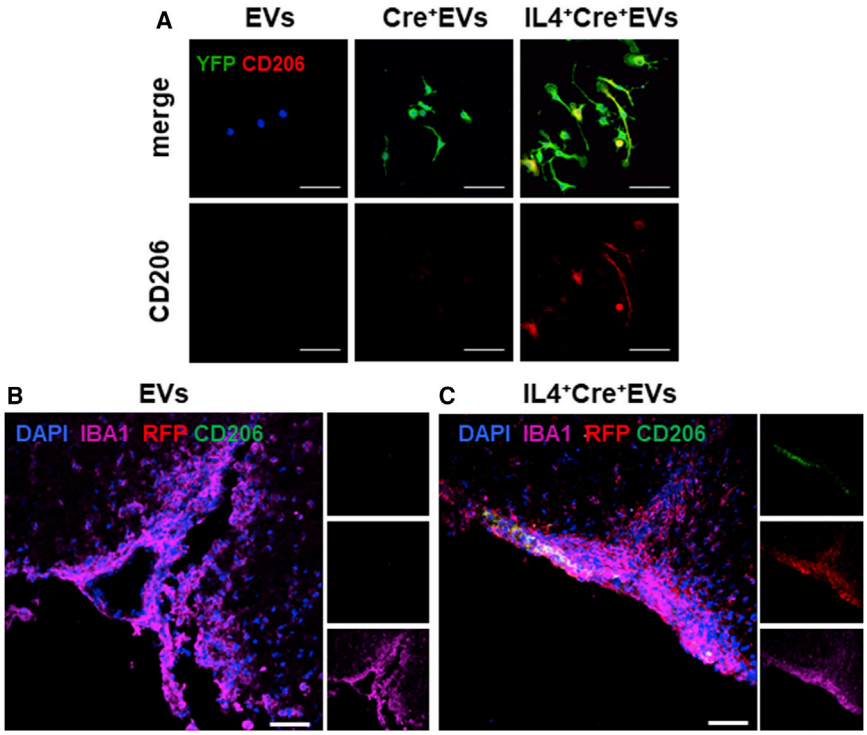

Figure 7. IL-4$^+$Mfg-e8$^+$ EVs Induce Anti-inflammatory Markers Only in Recipient Cells

(A) Immunofluorescence for YFP (green), CD206 (red), and DAPI (blue) on bone marrow macrophages from R26-stop-EYFP mice exposed for 24 hr to EVs, Cre$^+$ EVs, and IL-4$^+$Cre$^+$ EVs (n = 4). 60×; scale bar, 20 μm. (B and C) *In vivo*, IL-4$^+$Mfg-e8$^+$Cre$^+$ EVs induce the upregulation of the anti-inflammatory marker CD206 only in IBA1$^+$ cells that had recombined the reporter locus (C), compared to control EAE mice treated with IL-4$^-$Mfg-e8$^+$Cre$^+$ EVs (B); sections were stained for IBA1 (magenta), RFP (red), CD206 (green), and DAPI (blue). Magnification, 40×; scale bar, 50 μm; n = 3/group.

with patrolling activity and newly infiltrating phagocytes, such as monocyte-dendritic cells, which are extensively described as main effector cells in EAE.[30,31] As shown in Figures 6 and 7, using IL-4$^+$ EVs targeted with Mfg-e8, we can induce an anti-inflammatory phenotype in CD11b$^+$ cells, similar to gene therapy with IL-4.[14] Myeloid cells in the meningeal compartment and in the choroid plexus have been recently indicated as a crucial checkpoint in human and experimental neuroinflammation.[32–34] We and others[18] described in the past direct injection of rIL-4 in wild-type (WT) and EAE mice obtaining a very low effect (data not shown). The use of EVs to deliver IL-4 may increase its half-life and, therefore, its therapeutic effect. As we have shown, a single injection of 10^7 IL-4$^+$Mfg-e8$^+$ EVs has modulated established neuroinflammation, significantly reduced the clinical symptoms in EAE mice, and resulted in the prolonged modulation of recipient phagocytes toward an anti-inflammatory phenotype and in the inhibition of clinical and pathological signs of neuroinflammation.

In conclusion, our data support EVs' ability to deliver multiple signals (in our case IL-4, Cre, and Mfg-e8), both as protein and mRNA, a feature that opens a plethora of possibilities from the therapeutic point of view.

MATERIALS AND METHODS

Cells

BV-2 cells, primary microglia, and bone marrow and peritoneal macrophages were cultured in DMEM (Gibco) supplemented with 10% fetal bovine serum (FBS), penicillin, streptomycin (100 U/mL), and 2 mM L-glutamine.

EV Purification by Differential Ultracentrifugation

EVs were purified from the cell media using a standardized protocol[35] with slight modifications: conditioned cell supernatants were collected and centrifuged for 10 min at 300 × *g* to remove floating cells and debris. The resulting supernatants were further cleared through a 0.45-μm syringe filter (Millex, Millipore), then ultra-centrifuged at 100,000 × *g* for 1 hr to pellet EVs. Pellets were suspended in lysis buffer with protease inhibitor, PBS, or fixative depending on the specific aim. As serum contains high levels of EVs, cells were cultured in DMEM supplemented with EV-depleted serum.

EV Quantification by TRPS

Purified EVs were re-suspended in filtered PBS, and an aliquot (40 μL) was loaded onto a nanopore (NP200) previously activated by multiple washes with PBS. Recordings were performed with qNanoTM (Izon) using a voltage-pressure protocol, according to the manufacturer's instructions. Calibration particles (cpc200b, Izon) were used to define the dimensional range of the measured EVs.

EV Quantification by Flow Cytometry

EVs were stained with fluorescein isothiocyanate (FITC)-conjugated isolectin B4 from Bandeiraea Simplicifolia (Sigma-Aldrich). Calibration beads (BioCytex) of known dimensions (from 0.1 to 0.9 μm) were used to define the gate into which IB4$^+$ events can be considered as bona fide EVs. Samples were acquired using a Cytoflex analyzer (Beckman Coulter Genomics).

Cell Transfection

BV-2 cells were transfected with a lentiviral plasmid (p277.hPGK.IL-4, p277.hPGK.EGFP [kind gift of professor Luigi Naldini, San Raffaele Scientific Institute], 945hPGK.iCre-CMV.dNGFR, LV. F-GFP, and p.hPGK.Luciferase [kind gift of professor Giuliana Ferrari, San Raffaele Scientific Institute]) using lipofectamin (LTX, Invitrogen/Life

Technologies). Briefly, about 2×10^6 donor cells were transfected with 10 μg plasmid DNA (pDNA) and LTX in completed DMEM supplemented with 10% EV-depleted FBS. The medium was then replaced with 10 mL fresh EV-depleted medium. EVs were purified from supernatants after 48–72 hr.

Mfg-e8 EV Pseudotyping

2×10^6 BV-2 cells were infected with the lentivirus Mfg-e8-IRES-EGFP (psd44-iGFP-MFG-E8-long, Addgene), at MOI 20, in completed DMEM supplemented with 10% EV-depleted FBS for 48 hr. Cells were then collected and subjected to WB, immunofluorescence (IF), and gene expression analysis or stored at −80°C.

Transmission Electron Microscopy

EVs were observed at transmission electron microscopy (TEM) after negative staining: cell media were fractionated by differential ultracentrifugation, and the resulting pellets were re-suspended in 20 μL PBS and adsorbed to 400-mesh formvar/carbon-coated 17 grid for 10 min at room temperature (RT). Adherent vesicles were stained with uranyl acetate and immediately observed at the electron microscope.

WB Analyses

30 μg proteins and 5–10 μg EVs were diluted with Laemmli buffer and loaded onto 8%–14% polyacrylamide gels. Purified EVs were re-suspended in lysis buffer supplemented with a protease and phosphatase inhibitor cocktail (Sigma-Aldrich). Protein concentrations were measured with bicinchoninic acid (BCA) assay (Micro BCA, Pierce). Anti-flotillin1 (BD Biosciences), mouse anti-β actin (Sigma), rabbit anti-Alix (Millipore), goat anti-hsp70 (Santa Cruz Biotechnology), mouse anti-COX-IV (Cell Signaling Technology), rabbit anti-pstat6 (Cell Signaling Technology), IL-4Rα (Santa Cruz Biotechnology), and rat anti-Mfg-e8 (R&D Systems) were used as primary antibodies.

IL-4$^+$ EV Biological Assay

3–5 $\times$ 10^5 BV-2 cells, primary microglia, and bone marrow and peritoneal macrophages were cultured in completed DMEM supplemented with 10% EV-depleted FBS, and they were plated with 1–5 $\times$ 10^6 IL-4$^+$ EVs collected from donor IL-4$^+$BV-2 for 4–24 hr. IL-4 EVs were used as a negative control and rIL-4 (5–20 ng/mL, R&D Systems) as a positive control. Finally, cells were re-suspended in 500 μL Trizol (Invitrogen, Paisley, UK) for gene expression analysis or in 100 μL lysis buffer for WB.

Mfg-e8-Neutralizing Assay

3–5 $\times$ 10^5 BV-2 cells were cultured in completed DMEM supplemented with 10% EV-depleted FBS and plated with 1–5 $\times$ 10^6 IL-4$^+$Mfg-e8$^+$ EVs, IL-4$^+$ EVs, Mfg-e8$^+$ EVs, and empty EVs (without IL-4 and Mfg-e8), pre-treated or not with rαVβ5 integrin (5 ng/mL, R&D Systems), for 8–12 hr. Cells were re-suspended in Trizol (Invitrogen, Paisley, UK) for gene expression analysis.

IL-4$^+$Cre$^+$ EV Biological Assay

15 $\times$ 10^5 bone marrow macrophages collected from R26-stop-EYFP were cultured in completed DMEM supplemented with 10% EV-depleted FBS, and they were plated with 1 $\times$ 10^6 IL-4$^+$Cre$^+$ EVs or Cre-EVs for 24 hr. Cells were collected for IF analysis.

IL-4Rα-Blocking Assay

3–5 $\times$ 10^5 BV-2 cells were cultured in the presence or not of IL-4Rα-neutralizing antibody (1 μg/mL, R&D Systems), in completed DMEM supplemented with 10% EV-depleted FBS, and they were plated with 1–5 $\times$ 10^6 IL-4$^+$ EVs or IL-4 EVs pre-treated with IL-4Rα-neutralizing antibody (1 μg/mL) for 8–12 hr. rIL-4 (5–10 ng/mL) was used as a positive control. Cells were collected for IF analysis or re-suspended in Trizol (Invitrogen, Paisley, UK) for gene expression analysis.

Stat6 Inhibition Assay

3–5 $\times$ 10^5 BV-2 cells were cultured in the presence or not of stat6 pharmacological inhibitor AS1517499 (10 nM), Axon in completed DMEM supplemented with 10% EV-depleted FBS, and they were plated with 1–5 $\times$ 10^6 IL-4$^+$ EVs or IL-4 EVs for 4 hr. rIL-4 (5–10 ng/mL) was used as a positive control. Cells were re-suspended in Trizol (Invitrogen, Paisley, UK) for gene expression analysis.

Lysosome Inhibition Assay

3–5 $\times$ 10^5 BV-2 cells were cultured in the presence or not of Bafilomycin, a pharmacological inhibitor of lysosome acidification (1 μM, Sigma-Aldrich), in completed DMEM supplemented with 10% EV-depleted FBS, and they were plated with 1–5 $\times$ 10^6 IL-4$^+$ EVs or IL-4 EVs for 3–9 hr. rIL-4 (5–10 ng/mL) was used as a positive control. The cells were re-suspended in Trizol (Invitrogen, Paisley, UK) for gene expression analysis.

ELISA for Murine IL-4 and Mfg-e8

Murine IL-4 and Mfg-e8 were measured in conditioned media and in CSF using a DUO set ELISA (R&D Systems).

Fluorescence Microscopy

BV-2 cells, primary microglia, and macrophages were fixed with 4% paraformaldehyde (10 min at 4°C), quenched with 0.1 M glycine, and processed for indirect IF. A Leica SP5 (Leica Microsystems, Milan, Italy) confocal microscope and a GE Healthcare Delta Vision were used for image acquisitions. Images were analyzed with ImageJ software (NIH). Anti-IBA1 (Wako Pure Chemicals Industries), anti-INOS (Becton Dickinson), anti-Arginase1 (GeneTex), anti-CD206 (R&D Systems), and anti-GFP/YFP (Abcam) were used as primary antibodies.

Animals

6- to 8-week-old C57BL/6 female mice were purchased from Charles River Laboratories (Calco, Italy). R26-stop-dtTomato and R26-stop-EYFP mice were available in house.[36,37] All mice were housed in specific-pathogen-free conditions, in roomy cages, allowing free access to food and water with a constant light/dark cycle. All efforts

were made to minimize animal suffering and to reduce the number of mice used, in accordance with the European Communities Council Directive of November 24, 1986 (86/609/EEC). All procedures involving animals were performed according to the animal protocol guidelines prescribed by Institutional Animal Care and Use Committee (IACUC 644) at San Raffaele Scientific Institute (Milan, Italy).

IL-4 EV Therapy of EAE Mouse Model

Chronic EAE was induced in female C57BL/6 mice and R26-stop-dtTomato mice by subcutaneous injection of 300 μL of an emulsion containing 200 μg $MOG_{35–55}$ in Incomplete Freund's Adjuvant (IFA) (Sigma) supplemented with 8 mg/mL Mycobacterium tuberculosis (strain H37Ra; Difco, Lawrence, KS, USA). Pertussis toxin (500 ng, List Biological Laboratories, Campbell, CA, USA) was injected i.v. on the day of the immunization and again 2 days later. 10^7 GFP^+ EVs or IL-4^+ EVs were injected into the cisterna magna (i.c.) of the mice the day of clinical onset, as previously described.[14] Mice were weighed and scored for clinical signs daily up to the day of culling. Clinical assessment of EAE was performed according to the following scoring criteria: 0, healthy; 1, limp tail; 2, ataxia and/or paresis of hindlimbs; 3, paralysis of hindlimbs and/or paresis of forelimbs; 4, tetraparalysis; and 5, moribund or death.[38] EAE mice were killed at 30 and 45 days post-injection.

RT-PCR

Total RNA was extracted from EVs, BV-2 cells, primary microglia, macrophages, and from CNS-infiltrating cells of EAE mice with RNeasy Mini Kit (QIAGEN). Genomic DNA was removed by treatment with DNase I type (QIAGEN). cDNA synthesis was performed using Thermoscript RT-PCR system (Invitrogen). IL-4 (Mm00445259_m1), Arg1 (Mm00475988_m1), inos (Mm00440502_m1), ym1 (Mm00657889_mH), ifnγ (Mm01168134_m1), IL-17a (Mm00439618_m1), rorc (Mm00441144_g1), foxp3 (Mm00475156_m1), and gapdh (4352339E) mRNA levels were measured by real-time RT-PCR (Applied Biosystems, Invitrogen). The $2-\Delta\Delta CT$ method was used to calculate relative changes in gene expression.[39] Primers used for iCre cDNA analysis were as follows: forward, 5′-GCCTGCATTACCGGTCGATGCAACGA-3′; reverse, 5′-GTGGCAGATGGCGCGGCAACACCATT-3′.

Isolation of CNS-Infiltrating Leukocytes

Extracted brain and spinal cord tissues were incubated for 30 min with 0.4 mg/mL type IV collagenase (Sigma-Aldrich) and dissociated using a 19G syringe to obtain a homogeneous cell suspension. Finally, CNS cells were enriched by a Percoll gradient as previously described.[40]

CD11b$^+$ and CD4$^+$ Cell Separation

CNS-infiltrating leukocytes were spun at 300 × *g* for 10 min and then re-suspended in cold MACS Buffer (1× PBS, 0.5% BSA, and 2 mM EDTA). CD11b$^+$ and CD4$^+$ cells were isolated with a micro-beads kit (Miltenyi Biotec). Finally, cells were re-suspended in 500 μL TRizol (Invitrogen) and stored at –80°C.

Histological Evaluation

At least five mice per group were perfused through the left cardiac ventricle with saline plus EDTA 0.5 mM for 10 min, followed by fixation with cold 4% paraformaldehyde (PFA) (Sigma). Spinal cords and brains from EAE mice were dissected out and post-fixed in 2% PFA overnight. Four different stainings were used: H&E (inflammatory infiltrates), Kluver Barrera (demyelination), and Bielshowsky (axonal damage). Findings were quantified on an average of 10 complete cross-sections of spinal cord per mouse taken at eight different levels. The number of perivascular inflammatory infiltrates was calculated and expressed as the number of inflammatory infiltrates per square millimeter, and demyelinated areas and axonal loss were expressed as percentage of damaged area.

IF

IF was performed in brain and spinal cord sections of wild-type, mutant, and EAE mice. Briefly, CNS sections were washed two times with PBS1× and incubated in blocking solution PBS1×, 5% or 10% serum of secondary Ab species with or without Triton 0.1% (depending on the nature of the antigen), for up to 1 hr at room temperature. Primary antibodies were diluted in blocking mix (1% serum) and incubated at +4°C overnight, as suggested by the manufacturer's instructions. The following day CNS sections were rinsed in PBS1× three times for 5 min and fluorescent secondary antibodies (conjugated with Alexa Fluor 488, 546, or 644), diluted in blocking mix (1% serum). Slides were then washed three times in PBS1× for 5 min and incubated in DAPI for nuclei counterstaining (1:25,000; Roche Diagnostics Spa, Monza, Italy). The Leica SP5 and SP8 (Leica Microsystems, Milan, Italy) were used for image acquisitions. Images were analyzed with ImageJ software (NIH). Anti-IBA1 (Wako Pure Chemicals Industries), anti-INOS (Becton Dickinson), anti-Arginase1 (GeneTex), anti-luciferase (Abcam), and anti-GFP/YFP (Abcam) were used as primary antibodies.

EV Fate Mapping

8- to 10-week-old C57BL/6 female R26-stop-EYFP mice were injected i.c. with 10^7 EVs or with a lentivirus expressing luciferase (from professor Ferrari, San Raffaele Scientific Institute). Mice were monitored and sacrificed after 1 week for IF analysis.

BLI

Small animal BLI was performed by using the IVIS SpectrumCT System (PerkinElmer). Each mouse received an intraperitoneal injection of 150 mg luciferin/kg body weight 10 min before BLI. BLI was performed by acquiring a set of images every 2 min from 10 to 20 min after luciferin injection to detect the highest BLI signal (typically, 15 min post-injection). Images were obtained using the following IVIS settings: exposure time, auto; binning, 8; f, 1; and field of view, 13 cm (field C). No emission filters were used during BLI acquisitions. BLI analysis was performed by placing a region of interest (ROI) over the brain and by measuring the total flux (photons/s) within the ROI. Images were acquired and analyzed using Living Image 4.5 (PerkinElmer).

Statistical Analysis

Statistical evaluations are expressed as mean ± SD or mean ± SEM, as appropriate. Results were analyzed using one-way ANOVA, unpaired Student's t test, and Mann-Whitney U-test for samples with unknown and potentially disparate variances. Statistical significance was ranked as follows: *$p < 0.05$, **$p < 0.001$, ***$p < 0.0001$, and ****$p < 0.00001$.

SUPPLEMENTAL INFORMATION

Supplemental Information includes seven figures and can be found with this article online at https://doi.org/10.1016/j.ymthe.2018.06.024.

AUTHOR CONTRIBUTIONS

G.C. designed and performed the experiments and wrote the manuscript. F.C. contributed to *in vitro* experiments and revised the manuscript. A.F. contributed to EAE experiments. H.D. contributed to immunofluorescence and histological analyses and revised the manuscript. G.I.-R. contributed to pathological analysis and revised the manuscript. A.S. performed BLI. P.P. performed electron microscopy studies. M.B. contributed to fluorescence-activated cell sorting (FACS) analysis. G.M. contributed to the *in vivo* study design and revised the manuscript. L.M. contributed to the *in vitro* and *in vivo* study designs. R.F. supervised the study and wrote the manuscript. All authors read and approved the final manuscript.

ACKNOWLEDGMENTS

This work has been supported by Fondazione Italiana Sclerosi Multipla – FISM grant 2010/R/20 (R.F.) and an unrestricted grant from Merck (R.F. and L.M.). We are grateful to professors Luigi Naldini and Giuliana Ferrari for providing the lentiviral backbone and to Professor P. Brown for useful discussion.

REFERENCES

1. Théry, C., Ostrowski, M., and Segura, E. (2009). Membrane vesicles as conveyors of immune responses. Nat. Rev. Immunol. *9*, 581–593.
2. Porro, C., Trotta, T., and Panaro, M.A. (2015). Microvesicles in the brain: Biomarker, messenger or mediator? J. Neuroimmunol. *288*, 70–78.
3. Cocucci, E., Racchetti, G., and Meldolesi, J. (2009). Shedding microvesicles: artefacts no more. Trends Cell Biol. *19*, 43–51.
4. Mulcahy, L.A., Pink, R.C., and Carter, D.R. (2014). Routes and mechanisms of extracellular vesicle uptake. J. Extracell. Vesicles *3*.
5. Lässer, C., Théry, C., Buzás, E.I., Mathivanan, S., Zhao, W., Gho, Y.S., and Lötvall, J. (2016). The International Society for Extracellular Vesicles launches the first massive open online course on extracellular vesicles. J. Extracell. Vesicles *5*, 34299.
6. Fais, S., O'Driscoll, L., Borras, F.E., Buzas, E., Camussi, G., Cappello, F., Carvalho, J., Cordeiro da Silva, A., Del Portillo, H., El Andaloussi, S., et al. (2016). Evidence-Based Clinical Use of Nanoscale Extracellular Vesicles in Nanomedicine. ACS Nano *10*, 3886–3899.
7. Camussi, G., Deregibus, M.C., Bruno, S., Cantaluppi, V., and Biancone, L. (2010). Exosomes/microvesicles as a mechanism of cell-to-cell communication. Kidney Int. *78*, 838–848.
8. Lai, C.P., and Breakefield, X.O. (2012). Role of exosomes/microvesicles in the nervous system and use in emerging therapies. Front. Physiol. *3*, 228.
9. van Niel, G., D'Angelo, G., and Raposo, G. (2018). Shedding light on the cell biology of extracellular vesicles. Nat. Rev. Mol. Cell Biol. *19*, 213–228.
10. van der Vos, K.E., Abels, E.R., Zhang, X., Lai, C., Carrizosa, E., Oakley, D., Prabhakar, S., Mardini, O., Crommentuijn, M.H., Skog, J., et al. (2016). Directly visualized glioblastoma-derived extracellular vesicles transfer RNA to microglia/macrophages in the brain. Neuro-oncol. *18*, 58–69.
11. Zappulli, V., Friis, K.P., Fitzpatrick, Z., Maguire, C.A., and Breakefield, X.O. (2016). Extracellular vesicles and intercellular communication within the nervous system. J. Clin. Invest. *126*, 1198–1207.
12. Verderio, C., Muzio, L., Turola, E., Bergami, A., Novellino, L., Ruffini, F., Riganti, L., Corradini, I., Francolini, M., Garzetti, L., et al. (2012). Myeloid microvesicles are a marker and therapeutic target for neuroinflammation. Ann. Neurol. *72*, 610–624.
13. Poliani, P.L., Brok, H., Furlan, R., Ruffini, F., Bergami, A., Desina, G., Marconi, P.C., Rovaris, M., Uccelli, A., Glorioso, J.C., et al. (2001). Delivery to the central nervous system of a nonreplicative herpes simplex type 1 vector engineered with the interleukin 4 gene protects rhesus monkeys from hyperacute autoimmune encephalomyelitis. Hum. Gene Ther. *12*, 905–920.
14. Casella, G., Garzetti, L., Gatta, A.T., Finardi, A., Maiorino, C., Ruffini, F., Martino, G., Muzio, L., and Furlan, R. (2016). IL4 induces IL6-producing M2 macrophages associated to inhibition of neuroinflammation in vitro and in vivo. J. Neuroinflammation *13*, 139.
15. Hanayama, R., Tanaka, M., Miwa, K., Shinohara, A., Iwamatsu, A., and Nagata, S. (2002). Identification of a factor that links apoptotic cells to phagocytes. Nature *417*, 182–187.
16. Sun, D., Liu, F.J., Huang, R.B., and Zheng, L.S. (2011). Anionic heptadecanuclear silver(I) cluster constructed from in situ generated 2-mercaptobenzoic acid and a sulfide anion. Inorg. Chem. *50*, 12393–12395.
17. Kanada, M., Bachmann, M.H., Hardy, J.W., Frimannson, D.O., Bronsart, L., Wang, A., Sylvester, M.D., Schmidt, T.L., Kaspar, R.L., Butte, M.J., et al. (2015). Differential fates of biomolecules delivered to target cells via extracellular vesicles. Proc. Natl. Acad. Sci. USA *112*, E1433–E1442.
18. Pepe, G., Calderazzi, G., De Maglie, M., Villa, A.M., and Vegeto, E. (2014). Heterogeneous induction of microglia M2a phenotype by central administration of interleukin-4. J. Neuroinflammation *11*, 211.
19. Alvarez-Erviti, L., Seow, Y., Yin, H., Betts, C., Lakhal, S., and Wood, M.J. (2011). Delivery of siRNA to the mouse brain by systemic injection of targeted exosomes. Nat. Biotechnol. *29*, 341–345.
20. Kamerkar, S., LeBleu, V.S., Sugimoto, H., Yang, S., Ruivo, C.F., Melo, S.A., Lee, J.J., and Kalluri, R. (2017). Exosomes facilitate therapeutic targeting of oncogenic KRAS in pancreatic cancer. Nature *546*, 498–503.
21. Cossetti, C., Iraci, N., Mercer, T.R., Leonardi, T., Alpi, E., Drago, D., Alfaro-Cervello, C., Saini, H.K., Davis, M.P., Schaeffer, J., et al. (2014). Extracellular vesicles from neural stem cells transfer IFN-γ via Ifngr1 to activate Stat1 signaling in target cells. Mol. Cell *56*, 193–204.
22. Kurgonaite, K., Gandhi, H., Kurth, T., Pautot, S., Schwille, P., Weidemann, T., and Bökel, C. (2015). Essential role of endocytosis for interleukin-4-receptor-mediated JAK/STAT signalling. J. Cell Sci. *128*, 3781–3795.
23. Tibaldi, L., Leyman, S., Nicolas, A., Notebaert, S., Dewulf, M., Ngo, T.H., Zuany-Amorim, C., Amzallag, N., Bernard-Pierrot, I., Sastre-Garau, X., and Théry, C. (2013). New blocking antibodies impede adhesion, migration and survival of ovarian cancer cells, highlighting MFGE8 as a potential therapeutic target of human ovarian carcinoma. PLoS ONE *8*, e72708.
24. Takahashi, Y., Nishikawa, M., and Takakura, Y. (2017). In Vivo Tracking of Extracellular Vesicles in Mice Using Fusion Protein Comprising Lactadherin and Gaussia Luciferase. Methods Mol. Biol. *1660*, 245–254.
25. A-Gonzalez, N., Quintana, J.A., García-Silva, S., Mazariegos, M., González de la Aleja, A., Nicolás-Ávila, J.A., Walter, W., Adrover, J.M., Crainiciuc, G., Kuchroo, V.K., et al. (2017). Phagocytosis imprints heterogeneity in tissue-resident macrophages. J. Exp. Med. *214*, 1281–1296.
26. Martino, G., Furlan, R., Comi, G., and Adorini, L. (2001). The ependymal route to the CNS: an emerging gene-therapy approach for MS. Trends Immunol. *22*, 483–490.
27. Hudry, E., Martin, C., Gandhi, S., György, B., Scheffer, D.I., Mu, D., Merkel, S.F., Mingozzi, F., Fitzpatrick, Z., Dimant, H., et al. (2016). Exosome-associated AAV vector as a robust and convenient neuroscience tool. Gene Ther. *23*, 380–392.

28. Maguire, C.A., Balaj, L., Sivaraman, S., Crommentuijn, M.H., Ericsson, M., Mincheva-Nilsson, L., Baranov, V., Gianni, D., Tannous, B.A., Sena-Esteves, M., et al. (2012). Microvesicle-associated AAV vector as a novel gene delivery system. Mol. Ther. *20*, 960–971.

29. Ridder, K., Keller, S., Dams, M., Rupp, A.K., Schlaudraff, J., Del Turco, D., Starmann, J., Macas, J., Karpova, D., Devraj, K., et al. (2014). Extracellular vesicle-mediated transfer of genetic information between the hematopoietic system and the brain in response to inflammation. PLoS Biol. *12*, e1001874.

30. Croxford, A.L., Lanzinger, M., Hartmann, F.J., Schreiner, B., Mair, F., Pelczar, P., Clausen, B.E., Jung, S., Greter, M., and Becher, B. (2015). The Cytokine GM-CSF Drives the Inflammatory Signature of CCR2+ Monocytes and Licenses Autoimmunity. Immunity *43*, 502–514.

31. De Feo, D., Merlini, A., Brambilla, E., Ottoboni, L., Laterza, C., Menon, R., Srinivasan, S., Farina, C., Garcia Manteiga, J.M., Butti, E., et al. (2017). Neural precursor cell-secreted TGF-β2 redirects inflammatory monocyte-derived cells in CNS autoimmunity. J. Clin. Invest. *127*, 3937–3953.

32. Sie, C., and Korn, T. (2017). Dendritic cells in central nervous system autoimmunity. Semin. Immunopathol. *39*, 99–111.

33. Howell, O.W., Schulz-Trieglaff, E.K., Carassiti, D., Gentleman, S.M., Nicholas, R., Roncaroli, F., and Reynolds, R. (2015). Extensive grey matter pathology in the cerebellum in multiple sclerosis is linked to inflammation in the subarachnoid space. Neuropathol. Appl. Neurobiol. *41*, 798–813.

34. Schwartz, M., and Deczkowska, A. (2016). Neurological Disease as a Failure of Brain-Immune Crosstalk: The Multiple Faces of Neuroinflammation. Trends Immunol. *37*, 668–679.

35. Colombo, F., Bastoni, M., Nigro, A., Podini, P., Finardi, A., Casella, G., Ramesh, M., Farina, C., Verderio, C., and Furlan, R. (2018). Cytokines Stimulate the Release of Microvesicles from Myeloid Cells Independently from the P2X7 Receptor/Acid Sphingomyelinase Pathway. Front. Immunol. *9*, 204.

36. Srinivas, S., Watanabe, T., Lin, C.S., William, C.M., Tanabe, Y., Jessell, T.M., and Costantini, F. (2001). Cre reporter strains produced by targeted insertion of EYFP and ECFP into the ROSA26 locus. BMC Dev. Biol. *1*, 4.

37. Madisen, L., Zwingman, T.A., Sunkin, S.M., Oh, S.W., Zariwala, H.A., Gu, H., Ng, L.L., Palmiter, R.D., Hawrylycz, M.J., Jones, A.R., et al. (2010). A robust and high-throughput Cre reporting and characterization system for the whole mouse brain. Nat. Neurosci. *13*, 133–140.

38. Furlan, R., Cuomo, C., and Martino, G. (2009). Animal models of multiple sclerosis. Methods Mol. Biol. *549*, 157–173.

39. Livak, K.J., and Schmittgen, T.D. (2001). Analysis of relative gene expression data using real-time quantitative PCR and the 2(-Delta Delta C(T)) Method. Methods *25*, 402–408.

40. Ginhoux, F., Greter, M., Leboeuf, M., Nandi, S., See, P., Gokhan, S., Mehler, M.F., Conway, S.J., Ng, L.G., Stanley, E.R., et al. (2010). Fate mapping analysis reveals that adult microglia derive from primitive macrophages. Science *330*, 841–845.